Radiation Pattern Modeling with Characteristic Basis Function Patterns

Radiation Pattern Modeling with Characteristic Basis Function Patterns

André Young[(1)], Rob Maaskant[(2)], Marianna V. Ivashina[(2)], and David B. Davidson[(1)]
[(1)]Department of Electrical and Electronic Engineering, University of Stellenbosch, Stellenbosch, South Africa
(Email: ayoung@sun.ac.za; davidson@sun.ac.za)
[(2)]Department of Signals and Systems, Chalmers University of Technology, Gothenburg, Sweden
(Email: rob.maaskant@chalmers.se; marianna.ivashina@chalmers.se)

***Abstract*—The Characteristic Basis Function Pattern (CBFP) method is presented as a generic modeling technique for obtaining highly accurate approximations of antenna radiation patterns using very few measurements. The method is described in detail and illustrated for a reflector antenna system as an application example. Future challenges facing the further development and application of the method are also discussed.**

***Index Terms*—antenna radiation patterns, calibration, characteristic basis function patterns, radio astronomy.**

I. Introduction

The fast and accurate prediction of antenna radiation patterns is of importance in many wireless applications, ranging from antenna measurement to radar systems, and from earth observation to satellite antenna systems. In remote sensing applications, for instance, one attempts to remove the instrumental effects from the received signal in order to recover the true nature of the source of interest from that signal. This, in turn, requires an accurate characterization of the dominant instrumental effects at the time of observation as these effects manifest themselves in the antenna radiation pattern, which converts the incident electromagnetic waves into an electrical current at the antenna terminals. Often, the antennas used in such systems are exposed to harsh and highly variable environmental conditions, such as in space applications, aviation, and radio astronomy. In these instances, a once-off characterization of the system may be insufficient, since the instrumental effects vary, thus requiring routine calibration measurements to be performed at the time of observation. Furthermore, since instrumentation and signal processing techniques increase the receiving sensitivity even further, the required level of accuracy in determining the system response must increase as well in order to prevent instrumental effects from limiting the overall performance. This accuracy requirement should be balanced with the time allocated for performing the necessary calibration measurements as it reduces the time available for observation measurements.

The development of such efficient calibration techniques is currently a very active area of research within the radio astronomy community [1]–[4], since a new generation of instruments, such as MeerKAT [5], ASKAP [6], and the SKA [7], [8] are being developed. Utilising the sensitivity offered by these new systems to their full potential will require the use of so-called third-generation calibration methods which take into account direction-dependent (radiation pattern) effects over a wide angular region.

Ideally, the antenna directivity pattern should be accurately approximated by a model which can be expressed as a weighted sum of basis functions in which the weighting coefficients are the unknowns to be solved [9]. The basis functions used in the expansion should be chosen so as to minimize the number of terms required to reach a certain level of accuracy. Recently, various different approaches have been proposed as a solution to this beam calibration problem [10]–[14]. The common denominator in all these methods is the reliance on *a priori* knowledge of the antenna in consideration when choosing the basis functions. This is in no small part due to advances in computer technology and computational algorithms enabling the analysis of relatively large and complex antenna structures using rigorous full-wave methods [15], [16].

The Characteristic Basis Function Pattern (CBFP) method is one such approach [13], [14], [17]–[19], which constructs basis functions from measured and/or simulated radiation patterns for the antenna structure in question. The method distinguishes between a primary basis function pattern, which corresponds to an ideal realization of the antenna design (nominal pattern), and secondary CBFPs, each of which corresponds to a possible expected perturbation of the ideal antenna design. The high efficiency of this modeling approach is due to the fact that many of the pattern features are inherent to a particular antenna design and are therefore already included in the primary basis function giving a fairly accurate approximation to the radiation pattern of the actual antenna. Secondary basis functions are then included to optimally compensate for certain anticipated system errors that cause deviation of the radiation pattern from the ideally expected pattern.

A detailed description of the method is provided in the next section, followed by an illustrative example with numerical results in Section III. The final section discusses some future challenges concerning the application of the CBFP modeling method.

II. CBFP Method

In order to describe the CBFP method it is useful to view the antenna as a mathematical operator mapping a set of parameters defining its structure and operating point (e.g. dimensions, material properties and composition, array

excitation vector) to a single full-polarization complex-valued radiation pattern function defined on the far-field sphere [14]. Let there be a non-redundant set of N_d real-valued parameters that uniquely defines any particular instance of a given class of antennas. Each instance of the given antenna class may then be represented as an N_d-dimensional vector $\mathbf{d} \in \mathcal{D}$ where $\mathcal{D} \subseteq \mathbb{R}^{N_d}$. The far-field pattern function $\boldsymbol{p}(\theta, \phi)$ corresponding to the antenna instance $\mathbf{d}$ may then be determined via the mapping

$$Y : \mathcal{D} \to \mathcal{P} \tag{1}$$

so that $\boldsymbol{p}(\theta, \phi) = Y(\mathbf{d})$. The space $\mathcal{P}$ is defined as the set of all patterns that are realizable by selecting any $\mathbf{d}$ from $\mathcal{D}$, i.e. $\mathcal{P}$ is the image of $\mathcal{D}$ under Y.

For an ideal antenna the defining parameters are fixed to their designed values $\mathbf{d} = \mathbf{d}_0$ (or perfectly controlled in the case of a reconfigurable antenna), and the resulting radiation pattern can be determined exactly $\boldsymbol{p} = \boldsymbol{p}_0 = Y(\mathbf{d}_0)$. However, in practice, as a result of imperfect manufacturing processes and changing operating conditions, these antenna definition parameters may differ from their designed values, so that the actual realized instance $\mathbf{d}_r = \mathbf{d}_0 + \delta\mathbf{d}$, results in the realized radiation pattern $\boldsymbol{p}_r = \boldsymbol{p}_0 + \delta\boldsymbol{p}$, that is,

$$\boldsymbol{p}_r = \boldsymbol{p}_0 + \delta\boldsymbol{p} = Y(\mathbf{d}_0 + \delta\mathbf{d}) = Y(\mathbf{d}_r). \tag{2}$$

Note that in general $Y(\mathbf{d}_r) \neq \boldsymbol{p}_0 + Y(\delta\mathbf{d})$ due to the possible non-linearity in Y. Typically, there is some practical degree of uncertainty in measuring $\delta\mathbf{d}$, so that the resulting radiation pattern cannot be determined exactly.

However, in practice the variation in antenna configuration is limited so that for a particular design $\mathbf{d}_0$ the realizable configurations resides in a small subset $\mathcal{D}(\mathbf{d}_0) \subset \mathcal{D}$. Consequently any realized pattern $\boldsymbol{p}_r$ is an element of a subset $\mathcal{P}_r(\mathbf{d}_0) \subset \mathcal{P}$ centered around the nominal solution $\boldsymbol{p}_0$. Since the DOFs of the pattern perturbations is then physically limited, and since in practice the norm of the difference between the ideal and actual realized radiation patterns is relatively small, the CBFP assumes that any element in $\mathcal{P}_r$ can be approximated in a (K-dimensional) space $\mathcal{P}_B = \text{span}\{\boldsymbol{p}_k\}_{k=1}^K$ surrounding $\boldsymbol{p}_0$ and where each $\boldsymbol{p}_k \in \mathcal{P}_r(\mathbf{d}_0)$.

Hence, the CBFP method proceeds by finding a pattern model $\boldsymbol{p}_m$ such that $\boldsymbol{p}_r \approx \boldsymbol{p}_m$, where the approximation error is yet to be quantified through a suitable error norm, and where $\boldsymbol{p}_m$ itself is given through the expansion

$$\boldsymbol{p}_m(\theta, \phi) = \sum_{k=1}^{K} \alpha_k \boldsymbol{p}_k(\theta, \phi). \tag{3}$$

The set $\{\alpha_k\}_{k=1}^K$ contains the unknown expansion coefficients that need to be solved. Generally, $\boldsymbol{p}_r \notin \{\boldsymbol{p}_k\}_{k=1}^K$, since the differences between a given design and its realization are assumed to be unknown.

A. Generating Basis Functions Patterns

Since each of the pattern expansion functions $\{\boldsymbol{p}_k\}_{k=1}^K$ used in (3) is an element in $\mathcal{P}_r(\mathbf{d}_0)$, each pattern basis function corresponds to a different realization of a particular antenna design, i.e.,

$$\boldsymbol{p}_k(\theta, \phi) = Y(\mathbf{d}_k) \quad \text{for } k = 1, \ldots, K \tag{4}$$

where $\mathbf{d}_k = \mathbf{d}_0 + \delta\mathbf{d}_k$. It is pointed out that the mapping may not necessarily be unique, since different instances $\mathbf{d}$ can give rise to an identical radiation pattern if the radiation occurs from a structure that supports only a limited number of radiating modes (e.g. a single-mode radiating slot). Nonetheless, each of the relevant pattern basis functions can be obtained by applying a different perturbation to the antenna configuration and determining the resulting radiation pattern. Since $\mathbf{d}$ is an N_d-dimensional vector in a space spanned by N_d basis function vectors, we expect to generate also a corresponding set of N_d basis function patterns, implying that $K = N_d$. Any other instance $\mathbf{d}$ and its corresponding pattern is then obtained through the superposition principle. However, if Y is non-linear, the superposition principle does not hold and one must ensure to generate sufficient basis function patterns and therefore take the set $\{\mathbf{d}_k\}$ large, i.e., $K \gg N_d$. Evaluating Y is done through either simulation or, where possible, direct measurement. Note that the basis functions need to be constructed only once, even though the solution procedure for α_k in (3) may need to be repeated as often as necessary (typically once or more during the course of a single observation). This allows very accurate (potentially time-consuming) simulation or measurement techniques to be used in generating the basis functions without affecting the time required to perform the calibration measurements.

Let $\{\Omega_s\}_{s=1}^S$ be a set of S points on the far-field sphere where the radiation patterns are sampled to form each of the basis function patterns. Since the radiation pattern has two polarization components each of the basis functions may then be represented as a complex-valued $(2S)$-vector $\mathbf{p}_k$

$$\mathbf{p}_k = \begin{bmatrix} p_k^{(\text{CP})}(\Omega_1) \\ p_k^{(\text{CP})}(\Omega_2) \\ \vdots \\ p_k^{(\text{CP})}(\Omega_S) \\ p_k^{(\text{XP})}(\Omega_1) \\ p_k^{(\text{XP})}(\Omega_2) \\ \vdots \\ p_k^{(\text{XP})}(\Omega_S) \end{bmatrix} \tag{5}$$

where $p_k^{(\text{CP})}(\Omega_s)$ and $p_k^{(\text{XP})}(\Omega_s)$ are the co-polarized and cross-polarized components of $\boldsymbol{p}_k(\Omega_s)$, respectively. The discrete pattern model $\mathbf{p}_m$ constructed using the CBFP method may then be expressed as

$$\mathbf{p}_r \approx \mathbf{p}_m = \sum_{k=1}^{K} \alpha_k \mathbf{p}_k \tag{6}$$

where $\mathbf{p}_r$ is the actual radiation pattern of the antenna sampled over $\{\Omega_s\}$. Since the basis functions are generated once-off, the sampling used to construct them is made as dense as

required by the employed pattern interpolation scheme, so that the model (6) is able to predict the actual pattern in all desired directions sufficiently accurate.

Obtaining a useful set of basis functions requires proper selection of the perturbations $\delta\mathbf{d}_k$ that are applied to the antenna configuration in generating the radiation patterns. This in turn requires knowledge of the kind of differences that may be expected to be present between the actual antenna and its design. By systematically applying perturbations that form a set representative of the various expected possible antenna configurations a corresponding set of representative pattern functions is obtained.

For instance, the structure of a reflector antenna is known to differ from its design due to various environmental and manufacturing factors. Some of these differences may be deterministically related to specific causes, e.g., the structural deformation resulting from the gravitational loading associated with a specific pointing elevation angle. So a set of basis functions may be obtained by calculating the radiation pattern at a number of different elevations over the range of angles that the reflector will be steered to. The variation in the radiation pattern over the range of angles will generally be non-linear so that it may be insufficient to use only the patterns at the minimum and maximum elevations, and additional patterns obtained at intermediate elevations may be required. Now consider a second effect, say temperature induced panel buckling of the reflector surface. The resulting effect on the radiation pattern may be different from that due to varying gravitational loading so that the effectiveness of the basis functions constructed through varying the elevation angle may be limited when compensating for effects related to temperature variation. In this case more basis functions may need to be generated using different geometries that each corresponds to a different operating temperature.

As more effects are included the number of basis functions increases and more unknown coefficients need to be solved for in (6). Since it is desired to achieve the highest model accuracy for a given number of terms it is useful to form a set $\{\mathbf{u}_l\}_{l=1}^{L}$ of $L < K$ basis functions which can be used to accurately approximate any element in the space spanned by $\{\mathbf{p}_k\}_{k=1}^{K}$. It can be shown that such a set which minimizes the sum of squares of the distances from the space $\mathcal{U} = \operatorname{span}\{\mathbf{u}_l\}$ to each $\mathbf{p}_k$ is minimized by selecting $\{\mathbf{u}_l\}_{l=1}^{L}$ as columns from the matrix $\mathbf{U}$ where

$$\mathbf{P} = \begin{bmatrix}\mathbf{p}_1 & \mathbf{p}_2 & \cdots & \mathbf{p}_K\end{bmatrix} = \mathbf{U}\boldsymbol{\Sigma}\mathbf{V}^H \tag{7}$$

is the Singular Value Decomposition (SVD) of $\mathbf{P}$ [20]. The new set of basis functions is obtained by selecting the columns from $\mathbf{U}$ for which the singular values are above a certain tolerance $\tau \in [0, 1)$ relative to the maximum singular value. That is, for $\sigma_1 \geq \sigma_2 \geq \cdots \geq \sigma_L > \tau\sigma_1$ and $\tau\sigma_1 \geq \sigma_{L+1} \geq \sigma_{L+2} \geq \cdots \geq \sigma_K$ only the first L columns $\{\mathbf{u}_1, \mathbf{u}_2, \cdots, \mathbf{u}_L\}$ of $\mathbf{U}$ are retained as basis functions. The CBFP model constructed with orthonormalized basis functions then becomes

$$\mathbf{p}_r \approx \mathbf{u}_m = \sum_{l=1}^{L} \beta_l \mathbf{u}_l. \tag{8}$$

B. Pattern Model Solution

The model in (8) requires the solution of the expansion coefficients $\{\beta_l\}_{l=1}^{L}$. Toward this end, we first sample the actual radiation pattern and each of the basis functions in a few directions $\{\Omega_t\}_{t=1}^{T}$ with $T \geq L$, and where $T \ll S$, since the idea is to use as few measurements as possible. From this, the linear system

$$\mathbf{A}\boldsymbol{\beta} = \mathbf{y} \tag{9a}$$

is constructed with

$$y_t = p_r^{(P)}(\theta_t, \phi_t) \tag{9b}$$

and where A_{tl} is the element in $\mathbf{u}_l$ corresponding to polarization P and direction Ω_t. For $T = L$ pattern samples the system in (9) is exactly determined and a solution is found as $\boldsymbol{\beta} = \mathbf{A}^{-1}\mathbf{y}$; for $T > L$ the system is over-determined and a linear least-squares solution is obtained as $\boldsymbol{\beta} = \left(\mathbf{A}^H\mathbf{A}\right)^{-1}\mathbf{A}^H\mathbf{y}$. Since each of the basis functions defined in (5) contains both polarization components, a solution to the system (9) obtained using any combination of co- / cross-polarized samples of the actual pattern to form $\mathbf{y}$ will yield a full-polarization pattern model. However, practically it makes sense to use measurements of the co-polarized pattern if the antenna is designed to have low cross-polarization since this would typically yield a higher signal-to-noise ratio.

Since the radiation pattern is a complex-valued function the measurements used to construct $\mathbf{y}$ should also yield the phase pattern at the measured points. When the relative phase difference of the calibrator source is unknown from sample to sample, a correlation-based measurement can be used as described in [21]. In radio astronomy, for instance, this measurement technique involves a reference antenna that is pointed at a strong celestial calibrator radio source[1], while the antenna-under-test (AUT) is steered to position that same calibrator source successively at each of the directions $\{\Omega_t\}$ in which the radiation pattern is required to construct (9). The output voltages V_1 and V_2 of the reference antenna (#1) and the AUT (#2), respectively, are correlated to produce the correlation

[1]Often these sources are unpolarized, in which case the subsequent results are somewhat more complicated for a practical antenna with non-zero cross-polarization. It can be shown that under these conditions the correlation matrix elements become

$$R_{21} = \left\langle V_2^{(\mathrm{CP})}\overline{V}_1^{(\mathrm{CP})}\right\rangle + \left\langle V_2^{(\mathrm{XP})}\overline{V}_1^{(\mathrm{XP})}\right\rangle$$
$$R_{11} = \left\langle V_1^{(\mathrm{CP})}\overline{V}_1^{(\mathrm{CP})}\right\rangle + \left\langle V_1^{(\mathrm{XP})}\overline{V}_1^{(\mathrm{XP})}\right\rangle$$

where $V_i^{(\mathrm{CP})}$ ($V_i^{(\mathrm{XP})}$) is the voltage output produced by antenna i due to the component of the incident electric field which is parallel (orthogonal) to the co-polarization. The cross-terms that are omitted in the above expressions are zero since the two polarization components of the signal are uncorrelated, and both R_{11} and R_{21} contain one extra term which each affects the model solution in a different way. In R_{11} the added term is equivalent to a scalar multiplication of the right-hand side vector $\mathbf{y}$ in (9), whereas the added term in R_{21} is equivalent to additive noise which varies across the elements in $\mathbf{y}$ since the cross-polarized response of the AUT is a direction-dependent property [19]. However, if it may further be assumed that the reference antenna and AUT both have low cross-polarization, these expressions yield approximately the same result as (11) for the case where only co-polarized pattern measurements are performed.

It is assumed herein that the calibrator source is completely polarized and that it has the polarization that is defined as the co-polarization.

matrix $\mathbf{R}$. For a wide-sense stationary ergodic source signal the correlation may be replaced with a time-average, so that $\mathbf{R}$ may be written as

$$\mathbf{R} = \begin{bmatrix} R_{11} & R_{12} \\ R_{21} & R_{22} \end{bmatrix} = \begin{bmatrix} \langle V_1 \overline{V}_1 \rangle & \langle V_1 \overline{V}_2 \rangle \\ \langle V_2 \overline{V}_1 \rangle & \langle V_2 \overline{V}_2 \rangle \end{bmatrix} \tag{10}$$

where $\langle \cdot \rangle$ means the time-average and $\overline{x}$ means the complex-conjugate of x. With this result, the complex-valued radiation pattern samples can be obtained within a constant normalization factor, which can further be accounted for by calibrating on a source with known flux density. Then, the elements in the right-hand side vector in (9) become

$$y_t^{(P)} = \frac{R_{21}}{R_{11}} = \frac{p_r^{(P)}(\theta_t, \phi_t)}{p_{\text{ref}}^{(P)}(0,0)}. \tag{11}$$

After solving for the expansion coefficients $\boldsymbol{\beta}$, the pattern model in (8) can be used to predict the both polarizations of the actual radiation pattern in all directions $\{\Omega_s\}$ in which the basis functions are defined. Furthermore, if the sampling used to construct the basis functions is sufficiently fine, interpolation techniques can be used to obtain an accurate continuous beam model.

In evaluating the performance of the proposed modeling technique it is useful to consider the error between the actual pattern and the model. The accuracy of any given approximation to the actual radiation pattern is evaluated herein using the error metric

$$\text{Error} = \frac{\displaystyle\int_{\theta \le \theta_{\max}} \|\boldsymbol{p}_r - \boldsymbol{p}_m\|^2 \, \mathrm{d}\Omega}{\displaystyle\int_{\theta \le \theta_{\max}} \|\boldsymbol{p}_r\|^2 \, \mathrm{d}\Omega} \tag{12}$$

where $\theta_{\max}$ defines the relevant beam area centered around $(\theta = 0, \phi = 0)$. Since the pattern functions $\boldsymbol{p}_r$ and $\boldsymbol{p}_m$ are complex-valued this error takes into account differences in the phase patterns of the model and the actual pattern. Furthermore, since the pattern functions are also vector-valued, differences in both the co-polarized and cross-polarized components of the patterns also impact on the error.

Note that the solution to (9) does not guarantee the minimization of the error defined in (12) for a given set of model basis functions. An alternative method to determine the pattern model coefficients, which does minimize the error in (12), is to solve the system

$$\mathbf{A}'\boldsymbol{\beta} = \mathbf{y}' \tag{13a}$$

wherein

$$A'_{tl} = \int_{\theta \le \theta_{\max}} \boldsymbol{p}_l \cdot \overline{\boldsymbol{p}}_t \, \mathrm{d}\Omega \tag{13b}$$

$$y'_t = \int_{\theta \le \theta_{\max}} \boldsymbol{p}_r \cdot \overline{\boldsymbol{p}}_t \, \mathrm{d}\Omega. \tag{13c}$$

However, this solution for the model parameters is of little practical use, since the computation in (13c) requires knowledge of the actual radiation pattern over the entire angular region over which the model is to be used, thus defeating the purpose of seeking a model in the first place. Nevertheless, this approach is useful from a theoretical perspective and to test the efficiency of a given set of basis functions.

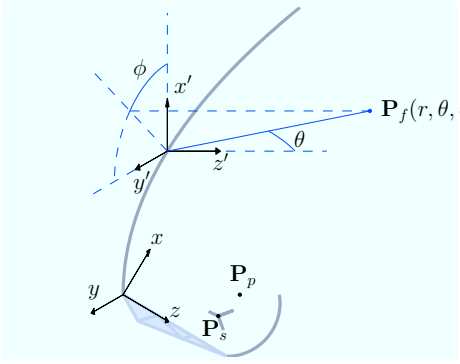

Fig. 1. Offset Gregorian reflector antenna. Positional errors of the feed and subreflector are referenced to the (x, y, z) coordinate system where z is directed along the support arm from the main reflector base to the subreflector base, x is in the symmetry plane. The far-field is referenced to the (x', y', z') coordinate system where z' is parallel to the main reflector axis and x' is in the symmetry plane.

III. Results

In this section, the CBFP modeling technique is illustrated through modeling the radiation pattern of a reflector antenna which, due to changing environmental and operating conditions, is varying in time. The antenna is a single-pixel fed offset Gregorian reflector with a projected diameter of 13.5 m and is based on the MeerKAT radio telescope [22]. Radiation patterns for the structure were obtained in GRASP [23] using Physical Optics and the Physical Theory of Diffraction (PO + PTD) principles. Unless stated otherwise, results are shown for an operating frequency of 1.42 GHz. Two kinds of structural deformations are assumed to affect the radiation pattern of the antenna, namely (see Fig. 1): (i) a deformation of the support arm, on which the feed and subreflector are hosted, and; (ii) a deformation of the main reflector surface.

A. Support arm deformation

In simulation, the deformation of the support arm is modeled by repositioning the feed and subreflector according to tolerances obtained from a mechanical analysis taking into account the effects of wind, temperature, and gravitational loading [24]. The range of expected positional errors for the feed and subreflector are listed in Table I. Since the feed and subreflector are fixed to the same support structure, the changes in their positions are affected in proportion to their relative positions on the support arm and the direction of change is the same for both components. Upon assuming that the rest of the system is free of errors, all possible realizations of the system can be described by the three-element row vector $\delta\mathbf{d} = [\delta_x\,,\,\delta_y\,,\,\delta_z]$ of normalized displacement positions, where $\mathbf{d} = \delta\mathbf{d}\,\mathbf{D}$ gives the absolute displacement of the subreflector from the designed position if $\mathbf{D}$ is a diagonal matrix such that $\mathrm{diag}\,(\mathbf{D}) = [0.01\,,\,0.005\,,\,0.02]$. Accordingly, we can define the subset $\mathcal{D}_r = \{(\delta_x, \delta_y, \delta_z)\,|\,\delta_x, \delta_y, \delta_z \in [-1, 1]\}$.

A few patterns from the corresponding $\mathcal{P}_r$ space obtained by varying δ_x are shown in Fig. 2. The patterns are shown in the xz-plane ($\phi = 0°$). The ideally expected pattern corresponds to the perfectly constructed antenna $\mathbf{d} = \mathbf{d}_0 = \mathbf{0}$, which has

Dimension	x [mm]	y [mm]	z [mm]
Feed	± 7.7	± 3.9	± 15.4
Subreflector	± 10.0	± 5.0	± 20.0

TABLE I
EXPECTED RANGE OF FEED AND SUBREFLECTOR POSITIONAL ERROR DUE TO SUPPORT ARM DEFORMATION.

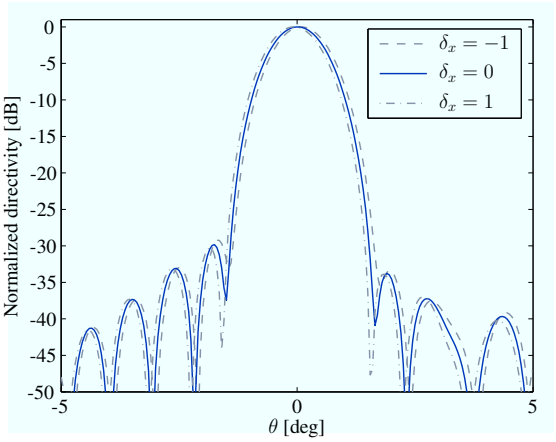

Fig. 2. Pattern variation resulting from x-displacement of the feed and subreflector.

$\delta_x = 0$, and the remaining two patterns correspond to the maximum displacement $\delta_x = \pm 1$ of the subreflector along the x-dimension. As expected, the feed (and subreflector) displacement primarily results in a change in the pointing direction of the main beam.

Suppose we wish to apply the CBFP method to model any pattern resulting from any $\delta_x \in [-1, 1]$. An obvious choice of basis functions is to use $Y(\mathbf{0})$ as the primary CBFP, and the two additional ones $Y([\pm 1\,,\,0\,,\,0])$ as secondary CBFPs. Using the SVD, an orthonormalized set of three basis functions is obtained to yield the model in (8). Now suppose the actual radiation pattern is $\boldsymbol{p}_r = Y([\delta_x\,,\,0\,,\,0])$ where $\delta_x = 0.4254$. The linear system in (9) is constructed by sampling the co-polarized component of $\mathbf{p}_r$ in three directions within the region $\theta \leq 1°$. This angular region is selected to be within the main beam region where the Signal-to-Noise Ratio (SNR) can be expected to be sufficiently high to yield accurate measurements. Next, the system model coefficient vector $\boldsymbol{\beta}$ is solved and the pattern model $\mathbf{u}_m$ is obtained. Fig. 3 shows the actual pattern and CBFP model, as well as the ideally expected pattern for comparison. On the scale shown, the model and the actual pattern are virtually indistinguishable in amplitude and phase, whereas the difference between the actual and expected pattern is clearly visible. The model also accurately predicts the pattern over a region covering the main lobe and first few sidelobes which extends well beyond the region within which the actual pattern was sampled.

Since Y is non-linear for the considered system, the range space $\mathcal{P}_r$ may be better approximated by generating more CBFPs, each of which corresponds to a basis function taken from a finer sampled domain space. Let the first space for x-displacements be $C_1^{(x)} = \{Y(\mathbf{d}) \mid \delta_x \in \Delta_1 \text{ and } \delta_y, \delta_z = 0\}$ where $\Delta_1 = \{0, \pm 1\}$ (the same as the set above), and then

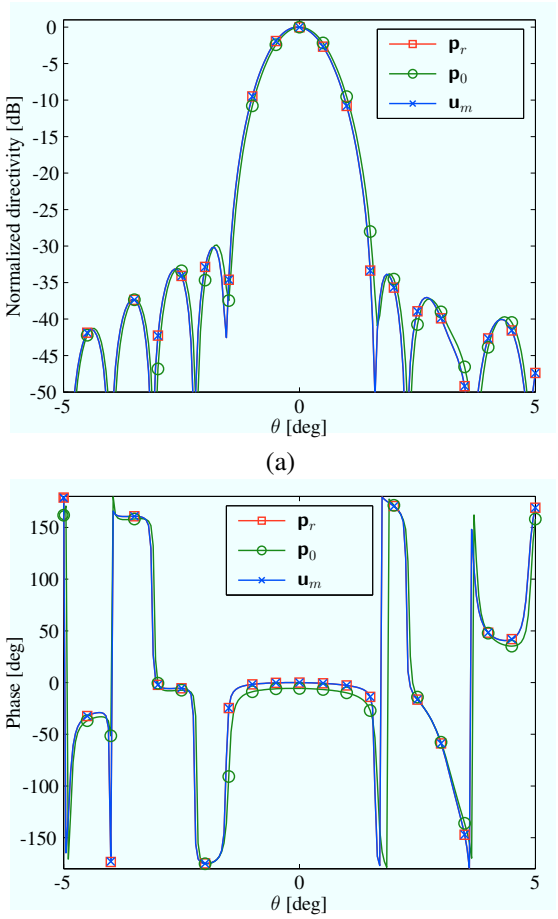

Fig. 3. CBFP model for x-displacement of the feed and subreflector. (a) Amplitude and (b) phase plots of the actual pattern $\mathbf{p}_r$, ideally expected pattern $\mathbf{p}_0$, and CBFP model $\mathbf{u}_m$ are all shown in the $\phi = 0°$ plane.

form similar sets $C_2^{(x)}$ and $C_3^{(x)}$ using $\Delta_2 = \{0, \pm 0.5, \pm 1\}$ and $\Delta_3 = \{0, \pm 0.25, \pm 0.5, \pm 0.75, \pm 1\}$, respectively. The SVD was performed for each of these sets, whose left-singular vectors corresponding to $\sigma_l \geq 10^{-6}\sigma_1$ were retained to form the new set of orthonormalized basis functions. This resulted in three basis functions for $C_1^{(x)}$ and five basis functions for both $C_2^{(x)}$ and $C_3^{(x)}$. Next, a number of CBFP models were solved for each set by varying the number of basis functions employed from that set and using in each case as many pattern samples within $\theta \leq 1°$ as there are unknown coefficients. The error in the model was then calculated using (12) and $\theta_{\text{max}} = 10°$. A comparison of the errors obtained with models containing various numbers of terms and constructed from the different sets is shown in Fig. 4(a). It is clear that finer samplings of the pattern space generally yield models of higher accuracy, even for a constant number of terms. Nevertheless, using only a two-term model from $C_1^{(x)}$ (and therefore sampling the actual pattern only in two directions) the error in the pattern model is already more than three orders of magnitude lower than the error in assuming the ideally expected pattern.

A similar result can be achieved for CBFP models to compensate for pattern variations resulting from a y-displacement

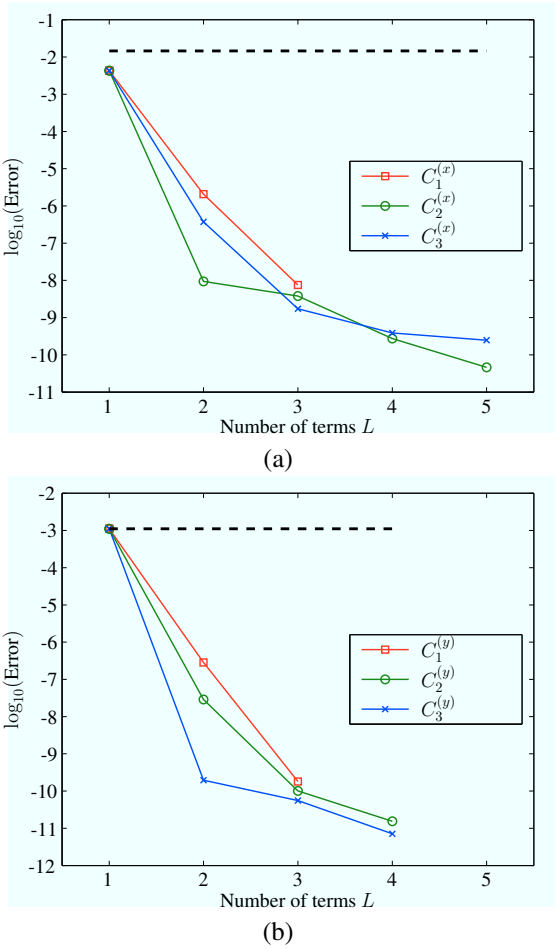

Fig. 4. CBFP model error as a function of the number of terms L. System error is (a) x-, and (b) y-displacement of the feed and subreflector. A comparison is shown for different sets of basis functions. Dashed horizontal line indicates error in assuming ideally expected pattern.

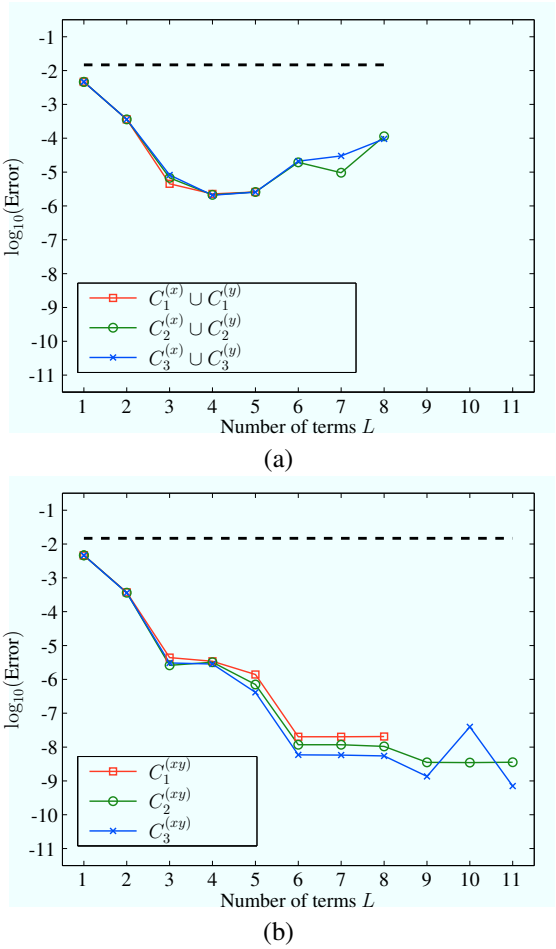

Fig. 5. CBFP model error as a function of the number of terms L. System error is xy-displacement of the feed and subreflector. A comparison is shown for different sets of basis functions constructed from (a) separate x- and y-displacement, and (b) separate as well as combined x- and y-displacement of the feed and subreflector. Dashed horizontal line indicates error in assuming ideally expected pattern.

of the feed and subreflector. In this case, the CBFP sets are $C_1^{(y)} = \{Y(\mathbf{d}) \,|\, \delta_y \in \Delta_1 \text{ and } \delta_x, \delta_z = 0\}$, as well as $C_2^{(y)}$ and $C_3^{(y)}$ similarly defined as before. The actual pattern to be modeled in this case is $\boldsymbol{p}_r = Y([0\,,\,\delta_y\,,\,0])$ where $\delta_y = 0.3914$. The errors in the various models are shown in Fig. 4(b). Note that the errors are typically smaller than for the case of x-displacements, and that using the same tolerance $\tau = 10^{-6}$ results in one less basis function to be retained in the sets $C_2^{(y)}$ and $C_3^{(y)}$ relative to the sets $C_2^{(x)}$ and $C_3^{(x)}$, respectively. This is a result of the fact that the range of positional errors is larger along the x- than the y-dimension.

Consider now generating a set of CBFPs to model pattern variations for displacement of the feed and subreflector in the xy-plane. One approach is to combine the sets constructed for the x- and y-displacements, e.g. $C_1^{(x)} \cup C_1^{(y)}$. However, owing to the non-linearity of Y this would not provide a very accurate approximation for any physically feasible solution in $\mathcal{P}_r$. A better approach would be to also employ CBFPs generated for displacements along both x and y simultaneously. Following this approach, let $C_1^{(xy)} = \{Y(\mathbf{d}) \,|\, (\delta_x, \delta_y) \in \Delta_1^2 \text{ and } \delta_z = 0\}$, and let $C_2^{(xy)}$ and $C_3^{(xy)}$ be similarly defined using $(\delta_x, \delta_y) \in \Delta_2^2$ and $(\delta_x, \delta_y) \in \Delta_3^2$, respectively. For the sake of comparison, both approaches are examined and models with various numbers of terms are constructed from the different sets as done above, and then solved, so that the errors for each model can be determined. The results are shown in Fig. 5(a) for the CBFP sets obtained by simply combining x- and y-displacement sets, and in Fig. 5(b) for CBFP sets that also contain patterns corresponding to simultaneous x- and y-displacements. From the results it is clear that the latter approach is preferred if high accuracy is priority — the addition of patterns for combined xy-displacement increases the dimension of the space spanned by the basis function set, and enables solutions of much higher accuracy. Nevertheless, for models with very few terms, either approach seems to yield similar levels of accuracy. In the case where these levels of accuracy are sufficient, the approach which simply combines x- and y-displacement sets is preferred since it typically requires much less initial CBFPs to be constructed.

Note in Fig. 5 that the addition of more basis functions to the model does not necessarily result in a decrease in error. In fact, in certain cases the error increases with addition of terms in

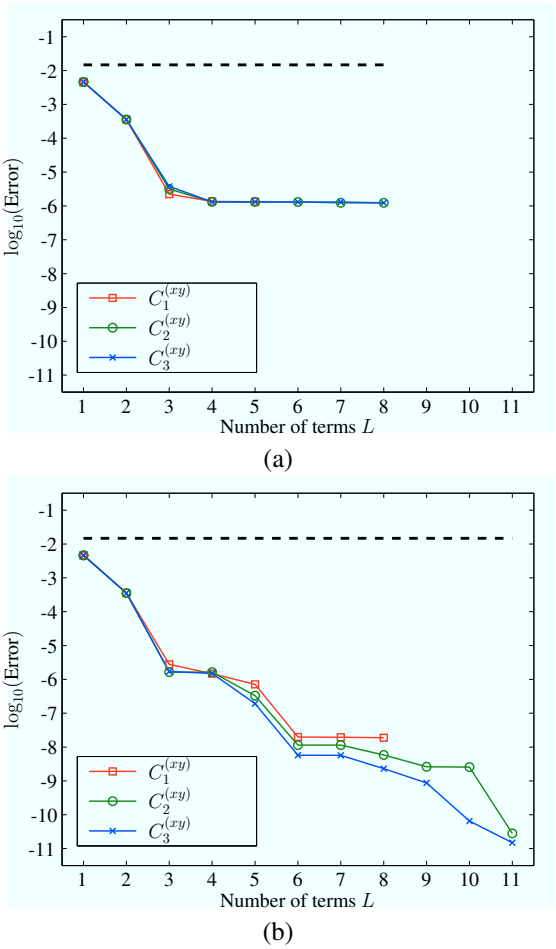

Fig. 6. Results similar to that in Fig. 5, except that the models are solved using the linear system in (13). A comparison is shown for different sets of basis functions constructed from (a) separate x- and y-displacement, and (b) separate as well as combined x- and y-displacement of the feed and subreflector. Dashed horizontal line indicates error in assuming ideally expected pattern.

the model. This is due to the fact that the solution to (9) does not guarantee the minimization of the error defined in (12) for a given set of model basis functions. Fig. 6 shows results similar to those in Fig. 5, except that the model solutions are obtained using (13) and with each additional term in the respective models the error is seen to decrease. However, in agreement with the results in Fig. 5, for larger numbers of basis functions the models which also employ CBFPs for simultaneous displacements along both x and y perform much better than those which simply combine CBFP sets for separate x and y displacement.

The difference between the actual pattern and each of the models obtained by solving (9) with $C_1^{(xy)}$ for $L = 1, 2, 3, 6$ is shown in Fig. 7. For comparison, the difference between the actual pattern and the ideally expected pattern is also shown. Differences are normalized to the maximum of the actual realized pattern. Using only one basis function ($L = 1$), a single testing point in the on-axis direction is used to solve the model, which results in a zero difference between the actual pattern and the model at that point. Adding the second basis function ($L = 2$) compensates for pattern variations similar to that observed for x-displacements, causing the pattern error to reduce significantly in the $\phi = 0°$ plane, while this is not really the case in the $\phi = 90°$ plane. Only after adding a third basis function ($L = 3$) the error in the $\phi = 90°$ plane reduces significantly. Not surprisingly, the orthonormalized basis functions obtained from the SVD are ordered in a specific manner to reflect the fact that a greater degree of pattern variation is observed for x- than for y-displacements, which is caused by the the larger range of movement allowed along the x-dimension for the considered mechanical deformations. Also note how the model accuracy for the cross-polarized component behaves as more basis functions are added. For the first two basis functions, the error for the cross-polarization component in the $\phi = 0°$ plane remains as high as that in the ideally expected pattern; this error only reduces from the third basis function upward. On the other hand, even employing the first basis function helps to reduce the error in cross-polarization level in the $\phi = 90°$ plane. For the offset design, the cross-polarization is practically zero in the plane of symmetry ($\phi = 0°$), but rather significant in the orthogonal plane ($\phi = 90°$). In the case where the subreflector and feed are displaced along the x-dimension, the symmetry is still intact and the cross-polarization level in the $\phi = 0°$ plane remains low, whereas a displacement along the y-dimension breaks the symmetry causing the cross-polarization level in that same plane to increase significantly. According to the ordering of the orthonormalized basis functions, as described above, this means that the second basis function, which compensates mostly for x-displacements, is unable to model relatively large cross-polarization levels in the $\phi = 0°$ plane. With the addition of the third basis function, which compensates mostly for y-displacements, the cross-polarization can be modeled properly in both planes.

Finally, the CBFP method was applied to model pattern variations resulting from displacements in all three dimensions and at two frequencies, viz., 580 MHz and 1750 MHz. The CBFPs that have been generated at both frequencies are $C^{(xyz)} = \{Y(\mathbf{d}) \,|\, (\delta_x, \delta_y, \delta_z) \in \Delta^3\}$ where $\Delta = \{0, \pm\frac{1}{3}, \pm\frac{2}{3}, \pm 1\}$. The orthonormalized basis functions for which $\sigma_l < 10^{-6}\sigma_1$ are yet again discarded. For the lower frequency, where the same absolute displacement is electrically smaller than at the higher frequency, only 9 CBFPs are retained; at the higher frequency 11 basis functions are retained. For each frequency, fifty actual patterns were then generated, each by applying an arbitrary displacement to the feed and subreflector within the space $\mathcal{D}_r$. Next, a CBFP model was developed for each of the resulting patterns using as many pattern measurements as there are solvable coefficients and by restricting these measurements to within the main beam region. Accordingly, the error was calculated for each model using $\theta_{\text{max}} = 13.2°$ and $\theta_{\text{max}} = 4.1°$ at the lower and higher frequency, respectively. The results are shown in Fig. 8(a) for the lower frequency and in (b) for the higher frequency. As can be expected, the overall error is smaller at the lower frequency than at the higher frequency. In either case, and for all solutions using only two basis functions, the model error is reduced to less than 10% between the actual and the ideally expected pattern.

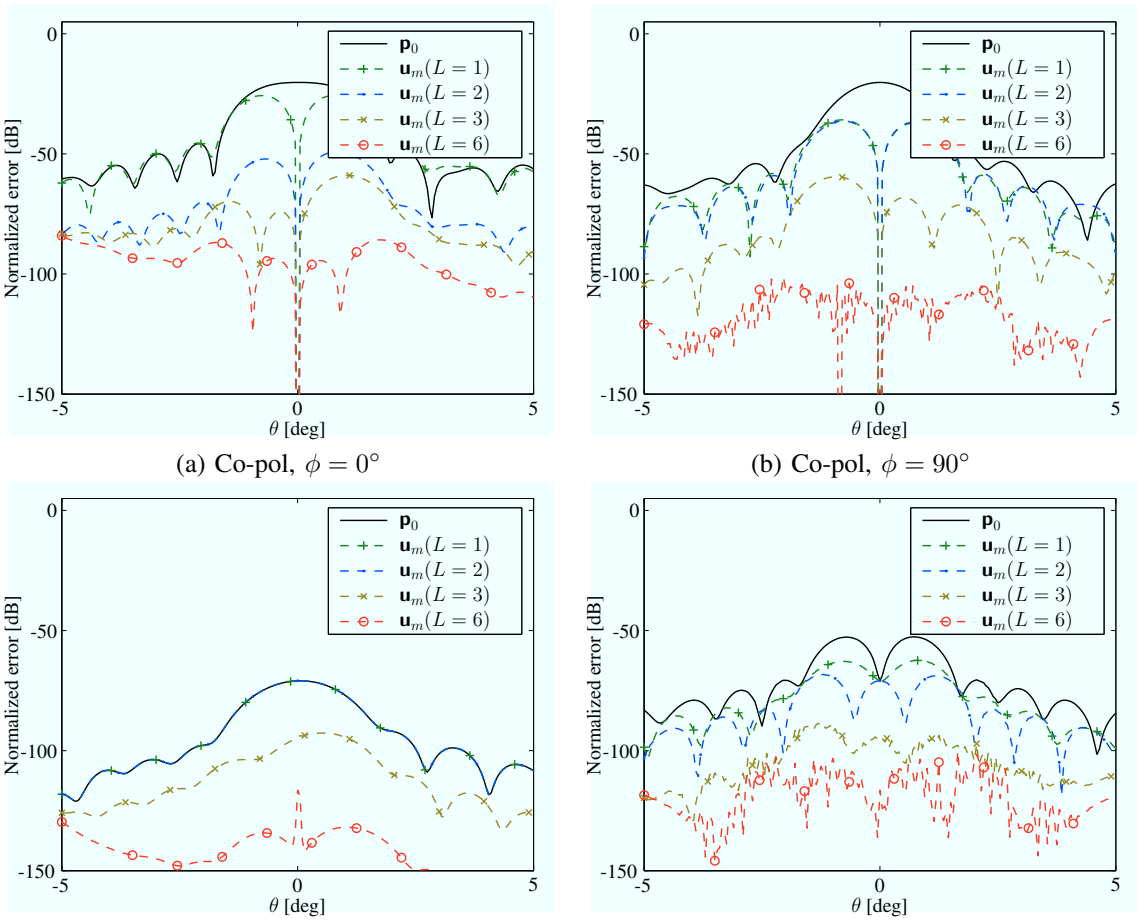

(a) Co-pol, $\phi = 0°$ (b) Co-pol, $\phi = 90°$

(c) Cross-pol, $\phi = 0°$ (d) Cross-pol, $\phi = 90°$

Fig. 7. Normalized difference between actual pattern and CBFP models with various numbers of terms. System error is xy-displacement of the feed and subreflector. Co-pol component shown in (a) $\phi = 0°$ and (b) $\phi = 90°$ planes, and cross-pol component shown in (c) $\phi = 0°$ and (d) $\phi = 90°$ planes. Difference between actual and ideally expected patterns is also shown.

B. Deformation of main reflector surface

The second kind of structural deformation considered here is that of the main reflector surface due to temperature variation. The reflector surface is assumed to consist of a number of panels that are arranged in concentric rings and divided sectorially. It is further assumed that the supporting structure on which the panels are mounted does not change with temperature, so that the edges of the panels (which are fixed to the underlying support structure) also remain in position. As the panels expand and contract with changes in the temperature the panels buckle, causing the reflector surface to deviate from a smooth paraboloid section. This effect is modeled in simulation by meshing the reflector surface into triangular patches and by applying an axial shift $\xi_{z'}$ to the mesh nodes according to the formula [19], [25]

$$\xi_{z'}(\rho,\psi) = \frac{\gamma\rho}{a}\left|\sin\left(m_\rho \pi \rho\right)\sin\left(\frac{m_\psi \psi}{2}\right)\right| \qquad (14)$$

where (ρ, ψ) are circular cylindrical coordinates over the main reflector aperture plane, a is the projected aperture diameter, m_ρ and m_ψ are the number of panels in the radial and angular directions, respectively, and γ is a temperature-dependent constant that controls the magnitude of the panel buckling. Compared to the formula used in [25], here a linear factor ρ is added to (14) to account for the large panel sizes farther out from the aperture center. Fig. 9 shows the surface error as a function over the aperture plane for $\gamma = 4.5 \times 10^{-3}$.

Assuming that this is the only error present in the system, all possible realizations of the antenna structure are entirely specified by the single parameter γ, which will here be limited to the range $[-\Gamma, \Gamma]$ with $\Gamma = 0.006$. The maximum surface error is therefore ≈ 6 mm, which is about $\lambda/35$ at 1.42 GHz. The corresponding space of realizable patterns $\mathcal{P}_r$ is then formed by the image of all mappings $Y(\delta_\gamma)$ where $\gamma = \Gamma\delta_\gamma$ and $\delta_\gamma \in [-1, 1]$.

The CBFP set constructed to compensate for the possible pattern variation was formed as $C^{(\gamma)} = \{Y(\delta_\gamma) \,|\, \delta_\gamma \in \Delta\}$ with $\Delta = \{0, \pm 0.5, \pm 1\}$ and the actual pattern to be modeled was obtained using $\boldsymbol{p}_r = Y(\delta_\gamma = 0.75)$. As before, only orthonormalized basis functions for which $\sigma_l \geq 10^{-6}\sigma_1$ are retained, resulting in only 4 CBFPs. Models with various numbers of terms were solved by sampling the actual pattern within the region $\theta \leq 1°$, and the error for each model was calculated using $\theta_{\text{max}} = 10°$.

The ideally expected pattern and a two-term CBFP model are compared to the actual pattern in Fig. 10. One observes that

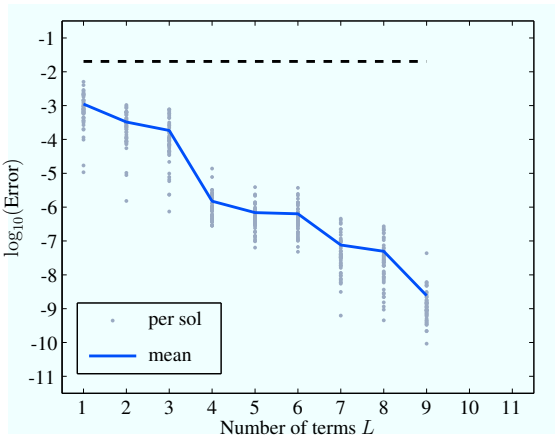

(a) 580 MHz

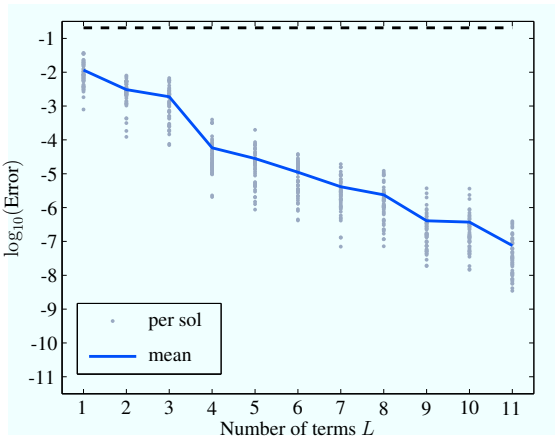

(b) 1750 MHz

Fig. 8. Error as a function of the number of basis functions L in each model at (a) 580 MHz and (b) 1750 MHz. System error is subreflector and feed xyz-displacement. Dots show results for fifty separate solutions and solid line indicates mean result across all fifty solutions. Dashed horizontal lines indicate error between ideally expected and actual patterns, averaged across all fifty solutions.

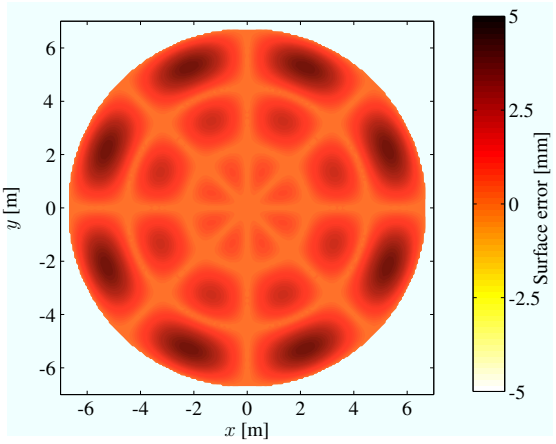

Fig. 9. Surface error over the aperture plane for $\gamma = 4.5 \times 10^{-3}$.

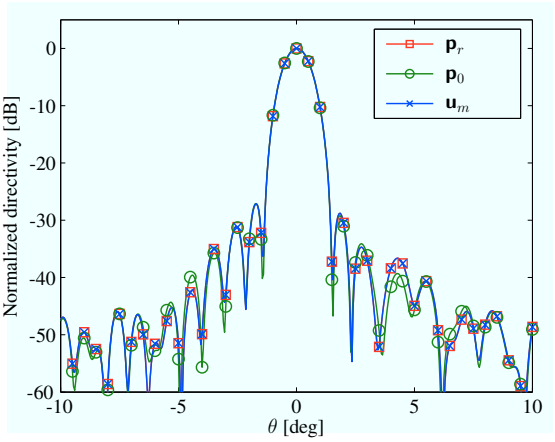

(a)

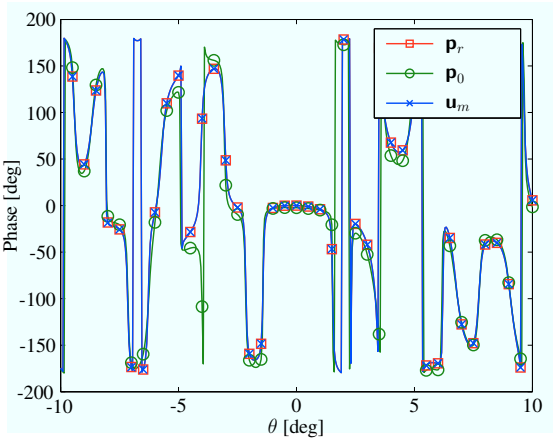

(b)

Fig. 10. Ideally expected pattern $\mathbf{p}_0$ and CBFP model $\mathbf{u}_m$ compared to actual pattern $\mathbf{u}_r$. (a) Amplitude and (b) phase patterns are shown in the $\phi = 20°$-plane. System error is temperature induced main reflector surface deformation.

the dominant effect on the radiation pattern of this particular deformation is a change in sidelobe structure, which the model is able to predict very accurately. The decrease in error, when the number of terms in the model is increased, is shown in Fig. 11, where the two-term model is seen to significantly reduce the error as compared to the error between the ideally expected and actual pattern.

IV. Discussion

This paper describes the CBFP method and demonstrates its use through examples pertaining to structural deformations typically occurring in a dual-reflector antennas. It has been shown that the actual realized pattern resulting from these system errors can be approximated accurately in a space of basis function patterns (CBFPs) of relatively low dimension. From this subspace of initially generated of CBFPs, highly accurate low-order (two- or three-term) CBFP models for these patterns can be extracted through the application of the SVD in conjunction with a threshold procedure on the singular values. This presents an efficient modeling solution in applications where the calibration of a time-varying radiation pattern using as few measurements as possible is required.

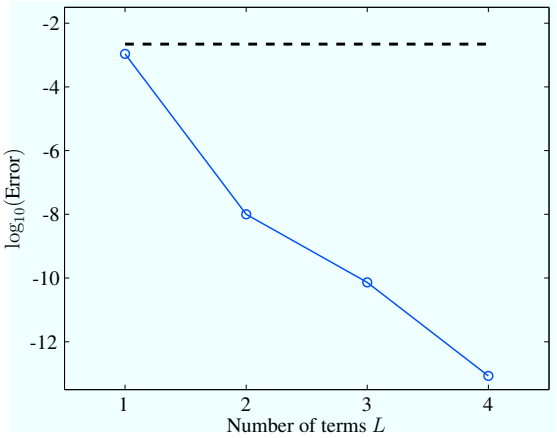

Fig. 11. Error as a function of number of terms L in the model. System error is temperature induced main reflector surface deformation. Dashed horizontal line indicates error between ideally expected and actual pattern.

In order to help put the results presented in this paper into perspective, it is useful to consider the accuracy requirement for certain applications. For example, in radio astronomy, achieving the image fidelity target of 10^{-4} for the SKA will require the root mean square error between the antenna radiation pattern and its model to be lower than about 5.5×10^{-3} for the dish array [14], [26]. Achieving this level of accuracy with traditionally used single-term analytic functions, such as the jinc-function[2] and $\cos^n$ functions [27]–[29], is impossible; even more sophisticated multiple-term analytic models do not offer sufficient accuracy [14], especially with as few terms as are typically used in the CBFP models presented herein. Meeting the requirements of an accurate pattern model, obtained with very few measurements at the observation time, will have to rely on approaches, such as the CBFP method proposed herein, where as much *a priori* knowledge of the antenna system is built into the model and only a few solvable parameters (DoFs) are retained to compensate for dominant sources of pattern variation.

In the following, some future challenges for the development and extension of the proposed CBFP method are discussed. Finally, some comments are made regarding the use of Macro Basis Functions (MBFs) and Nyquist sampling.

A. Extending Applications of the Method

Although the application example provided herein pertains to a certain class of expected system uncertainties affecting the beam pattern of reflector antennas, the extension of the method to other system errors and many other antenna designs is relatively straightforward. To this end, it is important to identify errors which are likely to be present in the system and which would have a significant effect on the radiation pattern. One application area where still much work is required is the beam modeling for large array antennas, such as for the LOFAR [30] radio telescope and the SKA-low [7]. The CBFP method was first demonstrated as an efficient calibration method for array antennas, where the element pattern was expected to perturb due to mismatch effects [13].

The major challenge is the sheer size of the arrays — on the order of a few hundred antenna elements. Even if the pattern of each of the antennas in the array is approximated with just a single-parameter model then, due to the size of the array, the model for the entire array would contain hundreds of solvable parameters, provided that one cannot use the array factor times the embedded element pattern approximation. In this case, it is necessary to develop techniques which could further reduce the number of solvable parameters in the model to find a practical beam modeling solution.

Another possible approach is to work directly with the array beam pattern when constructing basis functions. By doing this, the space in which the possible (array) antenna configurations reside becomes very large and it is yet to be determined how this affects the space of possible radiation patterns. Research in this direction is required to obtain an indication of how certain errors (e.g., weather dependent ground reflection, gain drift, etc.) in the array affect its radiation pattern.

Similar challenges exist for reflector antenna systems that employ dense array feeds or, so-called, "phase array feeds" (PAFs) [31], [32]. However, in this case the problem may exacerbate further as the presence of a complex reflector system may introduce an additional set of dominant system errors [33].

B. Experimental Verification

Thus far, results for the CBFP method have only been obtained through computer simulations, while the experimental verification of the accuracy of the method is still an important challenge to address. Firstly, it is to be determined how effective numerically generated CBFPs are at modeling the radiation pattern of an actual antenna. This is mostly determined by how well the physically built antenna can be characterized and modeled in simulation. In fact, precise causes for artifacts in the actual patterns can be hard to trace [26], which makes it difficult to introduce the relevant system errors in the simulation model when generating a set of CBFPs. This advocates the inclusion of at least one measured pattern in the set of CBFPs.

Secondly, suppose a CBFP model is constructed for an actual radiation pattern, then it is natural to question the accuracy of that model. Verifying the model accuracy would require the actual radiation pattern to be measured as it exists at the time when the model is solved. This may also prove challenging for large antenna structures (e.g., arrays or reflector antennas) since the radiation pattern has to remain stable during the course of a measurement.

C. Macro Basis Functions and Nyquist sampling

A question which has been raised (originally in the context of MBFs for frequency domain method of moments applications) is whether MBFs violate Nyquist sampling. This limit is often loosely specified as being $\lambda/2$, but this is only strictly valid in the context of explicit time-domain methods, such as the Finite Difference Time-Domain (FDTD) method. (In

[2]Similar to the naming of sinc function, $\text{jinc} = \frac{J_1(x)}{x}$ where J_1 is the 1st order Bessel function of the first kind.

the FDTD, for instance, the temporal sampling is defined by the Nyquist limit for a monochromatic analysis; in 1D, running at the Courant limit, this does indeed translate to a spatial sampling limit of $\lambda/2$.) For frequency domain methods, the appropriate Nyquist frequency is actually in the spectral (Fourier, or k-space) domain, and the appropriate frequency is spatial frequency. However, the key point here — in both the context of the MBF methods such as in computational electromagnetics and in the present context of patterns — is that since well-constructed MBFs inherently contain the required spatial variation, one can indeed apparently spatially under-sample. In particular in the present context, it is obvious that only one sample is needed if the solution is identical to the MBF. For this reason, MBFs have been generated in both the spectral and spatial domains [34], [35].

ACKNOWLEDGEMENT

The authors acknowledge the support of the South African Research Chairs Initiative of the Department of Science and Technology (DST) and National Research Foundation (NRF), as well as the Swedish VR and VINNOVA grants.

REFERENCES

[1] J. E. Noordam and O. M. Smirnov, "The MeqTrees software system and its use for third-generation calibration of radio interferometers," *Astronomy & Astrophysics*, vol. 524, p. A61, 2010.

[2] S. J. Wijnholds, S. van der Tol, R. Nijboer, and A. van der Veen, "Calibration challenges for future radio telescopes," *Signal Processing Magazine, IEEE*, vol. 27, no. 1, pp. 30–42, 2010.

[3] O. M. Smirnov, "Revisiting the radio interferometer measurement equation. II. Calibration and direction-dependent effects," *Astronomy & Astrophysics*, vol. 527, p. A107, 2011.

[4] ——, "Revisiting the radio interferometer measurement equation. III. Addressing direction-dependent effects in 21 cm WSRT observations of 3C 147," *Astronomy & Astrophysics*, vol. 527, p. A108, Mar. 2011.

[5] J. L. Jonas, "MeerKAT - The South African Array With Composite Dishes and Wide-Band Single Pixel Feeds," *Proc. IEEE*, vol. 97, no. 8, pp. 1522–1530, Aug. 2009.

[6] D. R. DeBoer, R. G. Gough, J. D. Bunton, T. J. Cornwell, R. J. Beresford, S. Johnston, I. J. Feain, A. E. Schinckel, C. A. Jackson, M. J. Kesteven *et al.*, "Australian SKA pathfinder: A high-dynamic range wide-field of view survey telescope," *Proc. IEEE*, vol. 97, no. 8, pp. 1507–1521, Aug. 2009.

[7] P. E. Dewdney, P. J. Hall, R. T. Schilizzi, and T. J. L. W. Lazio, "The Square Kilometre Array," *Proc. IEEE*, vol. 97, no. 8, pp. 1482–1496, Aug. 2009.

[8] The Square Kilometre Array. [Online]. Available: http://www.skatelescope.org

[9] J. E. Noordam, "Measuring Station Beamshapes as a function of time and frequency and in full polarization," in *3GC-II Workshop*, Albufeira (Portugal), Sep. 2011.

[10] C. Craeye, D. Gonzalez-Ovejero, E. de Lera Acedo, N. R. Ghods, and P. Alexander, "Main beam representation in non-regular arrays," in *CALIM*, Manchester (UK), Jul. 2011.

[11] C. Craeye, D. Gonzalez-Ovejero, N. R. Ghods, and E. de Lera Acedo, "A Projection Approach to Model the Main Beam of Non-Regular Arrays in Presence of Mutual Coupling," in *Proc. EuCAP*, Mar. 2012, pp. 2609–2612.

[12] E. de Lera Acedo, N. R.-G. D. Gonzalez-Ovejero, C. Raucy, and C. Craeye, "Low-Order Beam Models for Aperture Arrays," in *AACal*, Amsterdam (The Netherlands), Jul. 2012.

[13] R. Maaskant, M. V. Ivashina, S. J. Wijnholds, and K. F. Warnick, "Efficient Prediction of Array Element Patterns Using Physics-Based Expansions and a Single Far-Field Measurement," *IEEE Trans. Antennas Propag.*, vol. 60, no. 8, pp. 3614–3621, Aug. 2012.

[14] A. Young, "Improving the direction-dependent gain calibration of reflector antenna radio telescopes," Ph.D. dissertation, Stellenbosch University, Stellenbosch, South Africa, 2013. [Online]. Available: http://hdl.handle.net/10019.1/80915

[15] R. Maaskant, "Analysis of Large Antenna Systems," Ph.D. dissertation, Eindhoven University of Technology, Eindhoven, 2010. [Online]. Available: http://alexandria.tue.nl/extra2/201010409.pdf

[16] D. B. Davidson, R. Lehmensiek, D. I. L. de Villiers, and A. Young, "Current capabilities for the full-wave electromagnetic modelling of dishes for SKA," in *Proc. Int. Conf. on Electromagn. in Adv. Applicat. (ICEAA)*, Sep. 2013, pp. 1368–1371.

[17] R. Maaskant and M. V. Ivashina, "Characteristic Basis Function Patterns – A Novel Expansion Method for the Fast and Accurate Prediction of Antenna Array Beams," in *Proc. Int. Conf. on Electromagn. in Adv. Applicat. (ICEAA)*, Cape Town, Sep. 2012, pp. 796–799.

[18] A. Young, R. Maaskant, M. V. Ivashina, D. I. L. de Villiers, and D. B. Davidson, "Accurate Beam Prediction Through Characteristic Basis Function Patterns for the MeerKAT/SKA Radio Telescope Antenna," *IEEE Trans. Antennas Propag.*, vol. 61, no. 5, pp. 2466–2473, May 2013.

[19] A. Young, R. Maaskant, M. V. Ivashina, and D. B. Davidson, "Application of the characteristic basis function pattern method to reflector surface inaccuracies and sidelobe modeling," in *Proc. Int. Conf. on Electromagn. in Adv. Applicat. (ICEAA)*, Cape Town, Sep. 2013, pp. 555–558.

[20] I. Jolliffe, *Principal component analysis*. Springer, 1986.

[21] P. G. Smith, "Measurement of the Complete Far-Field Pattern of Large Antennas by Radio-Star Sources," *IEEE Trans. Antennas Propag.*, vol. 14, no. 1, pp. 6–16, Jan. 1966.

[22] I. Theron, R. Lehmensiek, and D. de Villiers, "The design of the MeerKAT dish optics," in *Electromagnetics in Advanced Applications (ICEAA), 2012 International Conference on*, Sep. 2012, pp. 539–542.

[23] TICRA. Copenhagen, Denmark. [Online]. Available: http://www.ticra.com

[24] A. Young, M. A. B. Terada, D. I. L. de Villiers, and D. B. Davidson, "Assessment of the Sensitivity of the South African KAT-7 and MeerKAT/SKA Radio Telescope Reflector Antennas," in *Proc. Int. Conf. on Electromagn. in Adv. Applicat. (ICEAA)*, Cape Town, Sep. 2012, pp. 486–489.

[25] A. Greve and D. Morris, "Repetitive radio reflector surface deformations," *IEEE Trans. Antennas Propag.*, vol. 53, no. 6, pp. 2123–2126, Jun. 2005.

[26] Harp, G. R. *et al.*, "Primary Beam and Dish Surface Characterization at the Allen Telescope Array by Radio Holography," *IEEE Trans. Antennas Propag.*, vol. 59, no. 6, pp. 2004–2021, Jun. 2011.

[27] A. Popping and R. Braun, "The standing wave phenomenon in radio telescopes," *Astronomy & Astrophysics*, vol. 479, no. 3, pp. 903–913, 2008.

[28] J. J. Condon, W. D. Cotton, E. W. Greisen, Q. F. Yin, R. A. Perley, G. B. Taylor, and J. J. Broderick, "The NRAO VLA Sky Survey," *The Astronomical Journal*, vol. 115, no. 5, pp. 1693–1716, 1998. [Online]. Available: http://stacks.iop.org/1538-3881/115/i=5/a=1693

[29] J. M. Uson and W. D. Cotton, "Beam squint and Stokes V with off-axis feeds," *A&A*, vol. 486, no. 2, pp. 647–654, 2008.

[30] M. De Vos, A. Gunst, and R. Nijboer, "The LOFAR Telescope: System Architecture and Signal Processing," *Proc. IEEE*, vol. 97, no. 8, pp. 1431–1437, Aug. 2009.

[31] A. Young, M. V. Ivashina, R. Maaskant, O. A. Iupikov, and D. B. Davidson, "Improving the Calibration Efficiency of an Array Fed Reflector Antenna through Constrained Beamforming," *IEEE Trans. Antennas Propag.*, vol. 61, no. 7, pp. 3538–3545, Jul. 2013.

[32] O. M. Smirnov and M. V. Ivashina, "Element gain drifts as an imaging dynamic range limitation in PAF-based interferometers," in *XXXth URSI General Assembly and Scientific Symposium*, Aug. 2011, pp. 1–4.

[33] S. .Wijnholds, M. V. Ivashina, R. Maaskant, and K. F. Warnick, "Polarimetry with phased array antennas: sensitivity and polarimetric performance using unpolarized sources for calibration," *IEEE Trans. Antennas Propag.*, vol. 60, no. 10, pp. 4688–4698, 2012.

[34] C. Craeye, "Finite-array characterization with the help of the ASM-MBF method: Eigenmode analysis," in *Electromagnetic Theory (EMTS), 2010 URSI International Symposium on*, Aug. 2010, pp. 168–170.

[35] J. Yeo, V. V. S. Prakash, and R. Mittra, "Efficient analysis of a class of microstrip antennas using the characteristic basis function method (CBFM)," *Micr. Opt. Technol.*, vol. 39, no. 6, pp. 456–464, 2003.

André Young was born in the Free State, South Africa on April 6, 1983. He received the B.Eng. degree in electrical and electronic engineering with computer science (*cum laude*), M.Sc.Eng. degree in electronic engineering (*cum laude*), and Ph.D. degree in electronic engineering in 2005, 2007, and 2013, respectively, from the University of Stellenbosch, Stellenbosch, South Africa. His master's thesis was on mesh termination schemes for the finite element method in electromagnetics and his doctoral dissertation was on direction-dependent gain calibration of radio telescopes.

He has worked on various engineering projects for Azoteq (Paarl, South Africa) and Entersekt (Stellenbosch, South Africa), and is currently appointed as a post-doctoral fellow at the University of Stellenbosch, where he was also appointed as a Junior Lecturer in 2009 and 2011. Since 2011 he has spent several months as a visiting researcher with the Antenna Group at the Chalmers University of Technology, Gothenburg, Sweden. His main research interests include signal processing for astronomical antenna arrays, antennas, and computational electromagnetics.

Rob Maaskant received his M.Sc. degree (*cum laude*) in 2003, and his Ph.D. degree (*cum laude*) in 2010, both in Electrical Engineering from the Eindhoven University of Technology, Eindhoven, The Netherlands. His Ph.D. has been awarded "the best dissertation of the Electrical Engineering Department, 2010." From 2003–2010, he was employed as an antenna research scientist at the Netherlands Institute for Radio Astronomy (ASTRON), Dwingeloo, The Netherlands, and from 2010–2012 as a postdoctoral researcher in the Antenna Group of the Signals and Systems Department at the Chalmers University of Technology, Sweden, for which he won a European Commission FP7 Marie Sklodowska-Curie Actions Outgoing – Rubicon Fellowship from the Netherlands Organization for Scientific Research (NWO), 2010. He is currently an Assistant Professor in the same Antenna Group. He is the primary author of the CAESAR software; an advanced integral-equation based solver for the analysis of large antenna array systems. His current research interest is in the field of receiving antennas for low-noise applications, meta-material based waveguides, and computational electromagnetics to solve these types of problems.

Dr. Maaskant received the 2nd best paper prize ('best team contribution') at the 2008 ESA/ESTEC workshop, Noordwijk, and was awarded a Young Researcher grant from the Swedish Research Council (VR), in 2011. He is an Associate Editor of both the IEEE Transactions on Antennas and Propagation and the FERMAT journal.

Marianna V. Ivashina received a Ph.D. in Electrical Engineering from the Sevastopol National Technical University (SNTU), Ukraine, in 2000. From 2001 to 2004 she was a Postdoctoral Researcher and from 2004 till 2010 an Antenna System Scientist at The Netherlands Institute for Radio Astronomy (ASTRON). During this period, she carried out research on an innovative Phased Array Feed (PAF) technology for a new-generation radio telescope, known as the Square Kilometer Array (SKA). The results of these early PAF projects have led to the definition of APERTIF - a PAF system that is being developed at ASTRON to replace the current horn feeds in the Westerbork Synthesis Radio Telescope (WSRT). Dr. Ivashina was involved in the development of APERTIF during 2008-2010 and acted as an external reviewer at the Preliminary Design Review of the Australian SKA Pathfinder (ASKAP) in 2009. In 2002, she also stayed as a Visiting Scientist with the European Space Agency (ESA), ESTEC, in the Netherlands, where she studied multiple-beam array feeds for the satellite telecommunication system Large Deployable Antenna (LDA). Dr. Ivashina received the URSI Young Scientists Award for the GA URSI, Toronto, Canada (1999), an APS/IEEE Travel Grant, Davos, Switzerland (2000), the 2nd Best Paper Award ('Best team contribution') at the ESA Antenna Workshop (2008) and the International Qualification Fellowship of the VINNOVA - Marie Curie Actions Program (2009) and The VR project grant of the Swedish Research Center (2010). She is currently an Associate Professor at the Department of Signals and Systems (Chalmers University of Technology). Her interests are wideband receiving arrays, antenna system modeling techniques, receiver noise characterization, signal processing for phased arrays, and radio astronomy. She is an Associate Editor of the IEEE Transactions on Antennas and Propagation and the FERMAT journal.

David Davidson David Bruce Davidson was born in London, U.K., 1961. He was raised and educated in South Africa, receiving the B.Eng, B.Eng (Hons), and M.Eng degrees (all cum laude) from the University of Pretoria, South Africa, in 1982, 1983, and 1986 respectively, and the Ph.D. degree from the University of Stellenbosch, Stellenbosch, South Africa, in 1991.

Following national service (1984-5) in the then South African Defence Force, he was with the Council for Scientific and Industrial Research, Pretoria, South Africa, prior to joining the University of Stellenbosch in 1988. As of 2011, he holds the South African Research Chair in Electromagnetic Systems and EMI Mitigation for SKA there. He was a Visiting Scholar at the University of Arizona in 1993, a Visiting Fellow Commoner at Trinity College, Cambridge University, England in 1997, a Guest Professor at the IRCTR, Delft University of Technology, The Netherlands, in 2003, and an Honorary Visitor, University of Manchester, UK in 2009. His main research interest through most of his career has been computational electromagnetics (CEM), and he has published extensively on this topic. He is the author of the recently revised text "Computational Electromagnetics for RF and Microwave Engineering" (Cambridge, U.K.: Cambridge Univ. Press, 1st edn, 2005, 2nd end, 2011). Recently, his interests have expanded to include engineering electromagnetics for radio astronomy.

Prof. Davidson is a Fellow of the IEEE, and a member of both the South African Institute of Electrical Engineers and the Applied Computational Electromagnetic Society. He is a recipient of the South African FRD (now NRF) Presidents Award; presently, he has a B2 research rating from the NRF. He received the Rectors Award for Excellent Research from the University of Stellenbosch in 2005. He is a Past Chairman of the IEEE AP/MTT Chapter of South Africa, served as an Associate Editor of the IEEE Antennas And Wireless Propagation Letters (06-08), and served on the IEEE Antennas and Propagation AdCom (11-13). He served as General Chair of the "8th International Workshop on Finite Elements for Microwave Engineering", held in Stellenbosch, May 2006. He was Chair of the local organizing committee of ICEAA-IEEE APWC-EEIS12, held in Cape Town in September 2012. Currently, he is the editor of the "EM Programmers Notebook" column of the IEEE Antennas And Propagation Magazine.